

# Dynamics of Trees of Fragmenting Granules in the Quiet Sun: *Hinode*/SOT Observations Compared to Numerical Simulation

J.M. Malherbe\*

*LESIA, Observatoire de Paris, 92195 Meudon, France*

T. Roudier†

*IRAP, Université de Toulouse, CNRS, CNES, 14 Avenue Edouard Belin, 31400 Toulouse, France*

R. Stein‡

*Physics and Astronomy Department, Michigan State University, East Lansing, MI 48824, USA*

Z. Frank§

*Lockheed Martin Solar and Astrophysics Laboratory,  
Palo Alto, 3251 Hanover Street, CA 94303, USA*

(Dated: August 27, 2018)

We compare horizontal velocities, vertical magnetic fields and evolution of trees of fragmenting granules (TFG, also named families of granules) derived in the quiet Sun at disk center from observations at solar minimum and maximum of the *Solar Optical Telescope* (SOT on board *Hinode*) and results of a recent 3D numerical simulation of the magneto-convection. We used 24-hour sequences of a 2D field of view (FOV) with high spatial and temporal resolution recorded by the SOT *Broad band Filter Imager* (BFI) and *Narrow band Filter Imager* (NFI). TFG were evidenced by segmentation and labeling of continuum intensities. Horizontal velocities were obtained from local correlation tracking (LCT) of proper motions of granules. Stokes  $V$  provided a proxy of the qline of sight magnetic field (BLOS). The MHD simulation (performed independently) produced granulation intensities, velocity and magnetic field vectors. We discovered that TFG also form in the simulation and show that it is able to reproduce the main properties of solar TFG: lifetime and size, associated horizontal motions, corks and diffusive index are close to observations. Largest (but not numerous) families are related in both cases to strongest flows and could play a major role in supergranule and magnetic network formation. We found that observations do not reveal any significant variation of TFG between solar minimum and maximum.

## I. INTRODUCTION

Roudier *et al.* (2016), referenced below as paper I, found from *Hinode* observations a relationship between the evolution of trees of fragmenting granules (TFG) and horizontal motions of magnetic features in the quiet Sun. They suggested that TFG could contribute to the formation of the magnetic network.

Reviews by Sheeley (2005) and Ossendrijver (2003) suggest that the quiet Sun contributes significantly to the solar magnetism. Understanding how magnetic fields form in the convective zone and are advected and diffused to the surface is a challenge which requires to investigate flows at various length scales (granulation, meso- and super-granulation), both from observations and MHD simulation (see review by Stein, 2012).

The solar granulation is organized in families of granules (TFG), which can live several hours. They are formed by successively exploding granules originating from a single parent (for the history of the discovery, please refer to paper I and Roudier *et al.*, 2003). We suspect TFG to be implied in network formation through mesoscale surface flows. Observations and simulations at similar space and time resolutions are necessary to characterize and understand their impact on magnetic elements.

In the present paper, the goal is to compare several *Hinode* observations at different dates along the cycle with an independent numerical simulation to examine how realistic it is in terms of TFG formation, evolution and interaction with magnetic elements. For this purpose, we analyze results coming out from several 24-hour sequences observed with *Hinode* (near solar minimum in 2007 and maximum in 2013, 2014) and the recent (2014) numerical simulation of magneto-convection based on Stein and Nordlund (1998). We study the dynamics of the solar surface at the mesoscale, relationships between TFG and horizontal motions, spatial power spectra, TFG size and lifetime, corks and diffusive index. We also investigate the action of TFG in the formation of the magnetic network.

## II. DESCRIPTION OF OBSERVATIONS AND PROCESSING METHODS

We used multi-wavelength data sets of the Solar Optical Telescope (SOT) on board *Hinode* (for a description of the SOT, see Ichimoto *et al.*, 2005; Suematsu *et al.*, 2008). The 0.50 m aperture of the SOT provides a spatial resolution of about  $0.25''$  (180 km) at 450 nm. Observations were done in the frame of HOP217 (determination

of the properties of families of granules and formation of the photospheric network) and HOP295 (connection of families of granules to the formation of the magnetic network). We observed at disk center, so that horizontal velocities can be derived from the proper motions of granules. Families can be detected from time evolution of granules.

For horizontal velocity measurements and TFG analysis, the BFI provided 24-hour sequences of the blue continuum at 450.4 nm. Observations were recorded continuously on 29-30 August 2007, from 10:48 to 10:40 UT and 30-31 August 2007 from 10:50 to 10:18 UT (two consecutive sequences, 2007a and 2007b, which can be combined to form a long 48 hours sequence). It must be noticed that the 2007 sequence is not far from a small remnant activity located south east. We also selected the 24-hour sequences of 28-29 April 2013, from 06:13 to 06:13 UT and 28-29 December 2014, from 22:14 to 22:56 UT (table).

After alignment of data (which reduced slightly the initial FOV), we applied a subsonic Fourier filter in the  $k-\omega$  space, where  $k$  and  $\omega$  are respectively the horizontal wave number and pulsation, in order to remove oscillations of continuum intensities. All Fourier components such that  $\omega \geq C_s k$  (where  $C_s = 6 \text{ km s}^{-1}$  is the sound speed and  $k = \sqrt{k_x^2 + k_y^2}$  is the horizontal wave number) were retained to keep only convective motions (Title *et al.*, 1989). In order to analyse TFG, we detected exploding granules and labeled them in time after segmentation as described by Roudier *et al.* (2003). Families or their different branches correspond to the mesogranular scale.

Horizontal velocities ( $v_x$  and  $v_y$ ) were also derived from aligned and filtered data of the blue continuum using the LCT technique (November and Simon, 1988, Roudier *et al.*, 1999) with a temporal window of 30 minutes and a spatial window of  $3.5''$ , providing mean motions at the mesoscale or larger. As such flows evolve slowly and families need at least 6 hours to develop, this explains why we worked with 24-hour sequences. The LCT is based on the detection of spatial and time-averaged granular proper motions. For vertical magnetic fields (BLOS), we used the NFI in shuttered Stokes  $I$  and  $V$  mode to record the  $V$  signal (a proxy of the magnetic field) in the blue wing of Fe I 630.2 nm (exposure time 0.12 seconds). The observations were recorded together with the BFI, at the same time and cadence. The Lyot filter was tuned to a single wavelength 12 pm apart from line core.  $I+V$  and  $I-V$  images were taken, then added or subtracted (providing respectively Stokes  $I$  and  $V$ ) on board the spacecraft. We also selected the long sequence of very quiet Sun in Na I D1 589.6 nm (shuttered  $V/I$  mode, exposure time 0.20 seconds) from 30 December 2008 (10:30 UT) to 5 January 2009 (05:37 UT) with 5 minutes time step which has a better sensitivity and a much lower JPEG type compression noise (table).

Instrument	$\lambda$ (nm)	Time step (s)	Pixel ( $''$ )	Duration (hours)	FOV ( $''$ )	Usage
BFI 2007	450.4	50.2	0.11	24	$112 \times 112$	LCT+TFG
BFI 2013	450.4	40.0	0.11	24	$84 \times 89$	LCT+TFG
BFI 2014	450.4	60.0	0.11	24	$77 \times 77$	LCT+TFG
IRIS 2015	283.2	60.0	0.17	6	$60 \times 60$	LCT
NFI 2007	630.2	50.2	0.16	24	$112 \times 112$	BLOS
NFI 2008	589.6	300	0.16	120	$112 \times 112$	BLOS

TABLE I. List of observations

### III. DESCRIPTION OF THE MHD SIMULATION

We used the results of the 3D magneto-convection stagger code which was run independently and not designed to model solar TFG. It solves the equations of mass, momentum and internal energy in conservative form plus the induction equation of the magnetic field, for compressible flow on a staggered mesh (Stein and Nordlund, 1998; Stein *et al.*, 2009; review by Stein, 2012). Solar rotation is included. Scalar variables (density, internal energy and temperature) are volume centered, momenta and magnetic field are face-centered, while currents and electric field are edge-centered. Time integration is performed by a 3rd order low memory Runge-Kutta scheme. Parallelization is achieved with MPI, communicating the three overlap zones that are needed in the 6th and 5th order derivative and interpolation stencils.

Boundaries are periodic horizontally and open at the top and bottom. The code uses a tabular equation of state that includes local thermodynamic equilibrium (LTE) ionization of the abundant elements as well as hydrogen molecule formation, to obtain the pressure and temperature as a function of log density and internal energy per unit mass. Radiative heating/cooling is calculated by explicitly solving the radiation transfer equation in both continua and lines assuming LTE. The number of wavelengths for which the transfer equation is solved is drastically reduced by using a multi-group method which accurately models the photospheric structure as revealed in line profiles and limb darkening.

Because the stagger code includes all the significant physical processes occurring near the solar surface and resolves the thin thermal boundary layer at the top of the convection zone, its results can be used to make predictions and be compared quantitatively with various solar observations, as oscillations (Rosenthal *et al.*, 1999; Stein and Nordlund, 2001), Fe I line formation (Asplund *et al.*, 2000), G band magneto-convection (Carlsson *et al.*, 2004), facular variability (De Pontieu *et al.*, 2006), velocities of magnetic elements (Langangen *et al.*, 2007), heliosismology (Zhao *et al.*, 2007) or correlation tracking (Georgobiani *et al.*, 2007). The initial state was a snapshot from a non-magnetic convective simulation. This in turn was the result of a series of hydrodynamic convec-

tion runs. All had the same 20 Mm depth. A 12 Mm wide simulation was run for two turnover times; then it was doubled three times to 96 Mm wide before the magnetic field was introduced (after 37.65 hours of hydrodynamic convection) as a 100 G uniform horizontal field, advected by inflows into the computational domain at the bottom. It took about 2 days (one turnover time) for significant magnetic flux to reach the surface.

Runs have dimensions  $2016 \times 2016 \times 500$  with resolution 48 km horizontally and 12-80 km vertically. Quantities at the visible surface were binned  $2 \times 2$  from 48 to 96 km ( $0.13''$  pixel size) to be comparable to observations ( $0.11''$ ). The physical parameters issued from the simulation are the emergent intensity, velocity field and magnetic field vectors (we used only horizontal velocities and the BLOS component). The FOV was  $131'' \times 131''$  and time step 60 seconds. The run duration covered a long time (100 hours), but we extracted a 26 hours sequence (start time: 59.5 hours; end time: 85.5 hours) for comparison to observations.

Several MP4 movies are joined as Electronic Supplemental Material (see the Appendix for details).

#### IV. HORIZONTAL VELOCITIES OF SIMULATION: COMPARISON BETWEEN PLASMA, LCT, FLCT AND CST

The numerical simulation provides the horizontal velocity vector over the 2D FOV during 26 hours with 60 seconds time step. It is a good opportunity to compare the plasma velocity to the one issued from indirect methods, such as LCT, FLCT (Fourier LCT, Fisher and Welsch, 2008) or CST (Coherent Structure Tracking, Rieutord *et al.*, 2007), applied to intensity structures as granules. FLCT compares two consecutive images while LCT and CST are time averaged. We used 30 minutes and  $3.5''$  averaging windows. Indeed Rieutord *et al.* (2001) showed that granules are good tracers of solar surface velocities for space and time scales not shorter than these typical values. In order to compare the quality of structure tracking to plasma motion, we applied the same windows to horizontal flows. Figure 1 shows that the correlation between plasma and LCT or FLCT velocities is morphologically good; this is not the case of the CST (which gives, on the contrary, much better results at  $1''$  resolution, see Roudier *et al.*, 2012). The next two figures provide quantitative results.

Figure 2 allows to compare performances of LCT, FLCT and CST for windows of 30 minutes/ $3.5''$ . We analysed the departures between the direction of horizontal velocities given by these methods and the plasma velocity vector (PLA), filtered by the same windows. The mean angle between LCT, FLCT, CST and PLA is almost null, but the dispersion is 3.75 times higher with the CST (standard deviation 34 degrees instead of 9 degrees for LCT or FLCT); the mean ratio between PLA and LCT velocity module is 2.0; while between PLA and

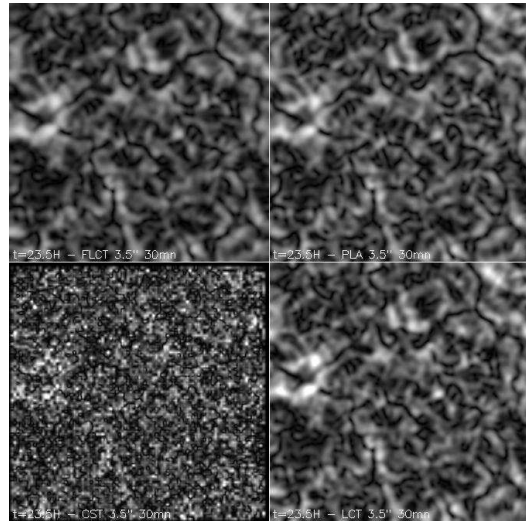


FIG. 1. Comparison between plasma, LCT, FLCT and CST horizontal velocity module using an averaging 30 minutes temporal window and  $3.5''$  spatial window. FOV =  $131'' \times 131''$ . Top left: FLCT velocity; top right: plasma velocity; bottom left: CST velocity; bottom right: LCT velocity

CST, or PLA and FLCT, we got respectively 1.15 and 1.12. The distribution function is definitely asymmetric for CST with an important tail. The best method is FLCT, but as it is slow for long sequences and large images, so we used the LCT instead to determine mesoscale horizontal flows, even if it underestimates the velocity module.

#### V. HORIZONTAL VELOCITIES FROM LCT: OBSERVATIONS AND SIMULATION

We now compare horizontal velocities provided by the LCT applied to *Hinode* observations and simulation. We also add a new Interface Region Imaging Spectrograph observation (IRIS, HOP312), performed on 10-11 October 2015 (23:34 to 05:32 UT) at disk center with the slit jaw (ultra violet continuum at 283.2 nm) with 13.8 seconds time step,  $0.166''$  pixel size and 6 hours duration sequence; the IRIS, *Hinode* and simulation data sets do not differ much in pixel size. We used the same temporal and spatial windows for all (30 minutes,  $3.5''$ ).

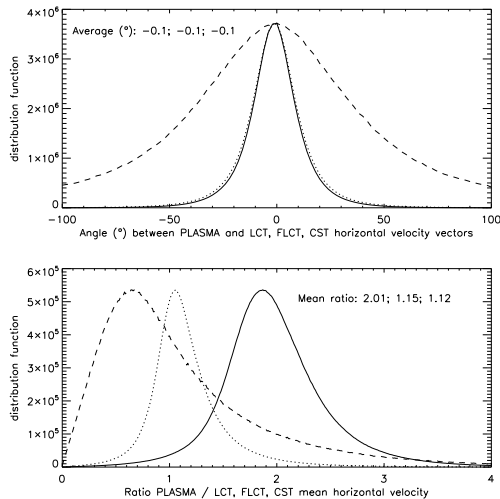


FIG. 2. Comparison of PLA, LCT, FLCT and CST horizontal velocities of simulation. Top: mean angle between velocity vectors (solid: PLA, LCT; dotted: PLA, FLCT; dashed: PLA, CST). Bottom: mean ratio between velocity modules (solid: PLA/LCT; dotted: PLA/FLCT; dashed: PLA/CST). Average values are indicated for direction and ratio.

Figure 3 shows, as a function of time, the behavior of the plasma velocity module and LCT proxy of the simulation, together with LCT velocity modules of *Hinode* (2007, 2013, 2014) and IRIS (2015). Velocities are averaged on the FOV and remain almost constant in time. If we apply a factor 2.0 to LCT observations, we find a mean horizontal velocity of 0.8 km/s, close to the 0.65–0.70 km/s of the simulation.

## VI. MAGNETIC FIELDS OF THE QUIET SUN

Figure 4 shows typical magnetic fields (BLOS) of *Hinode* 2007 and 2008 at disk center (0.16'' pixel size), together with the beginning and the end of the 26 hours numerical sequence (0.13'' pixel) extracted from the full run. The 2008 FOV shows several supergranular cells, but also that there exists a lot of spatially concentrated and mixed polarities inside cells, as noticed by Dominguez Cerdeña *et al.* (2006). The 2007 FOV is more noisy and contains a well structured supergranule with BLOS mainly South. The numerical simulation is

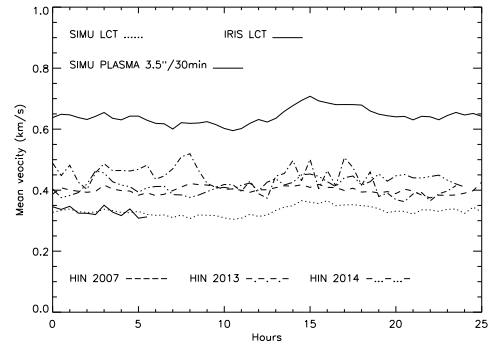


FIG. 3. Mean horizontal velocity over the FOV as a function of time. Solid line: plasma velocity (simulation); dotted line: LCT (simulation); dashed line: LCT *Hinode* 2007; dash-dot: LCT *Hinode* 2013; dash-dot-dot: LCT *Hinode* 2014; thick solid line: LCT IRIS 2015.

not magnetically steady state (there is a constant input of horizontal field at the bottom of the box); at the surface, there is more field at the end of the sequence than at the beginning. Polarities are much more mixed than in observations, with narrow concentrated flux tubes, so that it is not so easy to distinguish the network. As the spatial resolution of BLOS is much better in the simulation, we filtered it by the point spread function (PSF) of the SOT (including the 50 cm aperture, central occultation, spider and CCD, assuming no defocus). Orozco Suárez *et al.* (2007) pointed out the role of instrumental degradation for imaging magnetic fields with *Hinode*. The 2008 sequence (with the best magnetic sensitivity) exhibits a spatial distribution fairly close to the simulation, with well formed network and mixed polarities inside.

The distribution functions of the vertical magnetic field (Figure 5) exhibit an asymmetry between north and south polarities for *Hinode* 2007 (probably due to the vicinity of a weak active region). On the contrary, there is almost no asymmetry in 2008 (very quiet Sun region); polarities of the numerical simulation are well balanced but produce concentrated fields much more intense. In particular, BLOS is smaller than 200 Gauss for *Hinode*

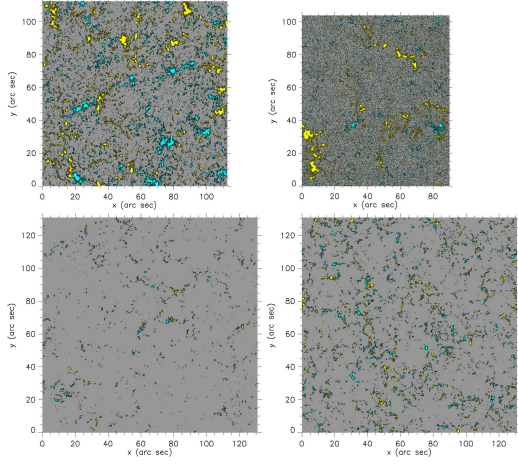


FIG. 4. Vertical magnetic field (blue/yellow for north/south polarities); top left: *Hinode* 2008; top right: *Hinode* 2007; bottom left: simulation start at 59.5 hours; bottom right: simulation end at 85.5 hours, filtered by the SOT PSF.

2007 (350 Gauss for 2008), while kilo Gauss (kG) fields are produced by the MHD code. However, Figure 5 shows that kG fields vanish when the SOT PSF is applied to the simulation. BLOS is likely underestimated by the Stokes sensitivity and the spatial resolution of the SOT and NFI filter.

In particular, the simulation reveals the presence of mainly vertical kG flux tubes only in intergranular lanes (median angle with the vertical 9 degrees, 90% of angles smaller than 17 degrees). The vertical velocity in flux tubes is downward ( $-2.23$  km/s in average). The downflow increases with magnetic field strength ( $-1.92$ ,  $-2.67$  and  $-3.43$  km/s respectively for fields above 1.0, 1.5 and 2.0 kG). 97% of flux ropes produce downdrafts. Unfortunately, the spatial resolution of *Hinode* does not allow to check these predictions.

## VII. SPATIAL POWER SPECTRA OF HORIZONTAL VELOCITIES

Figure 6 provides the power spectra of horizontal velocities of *Hinode*/BFI observations as well as the simulation. The power spectrum is defined as the square mod-

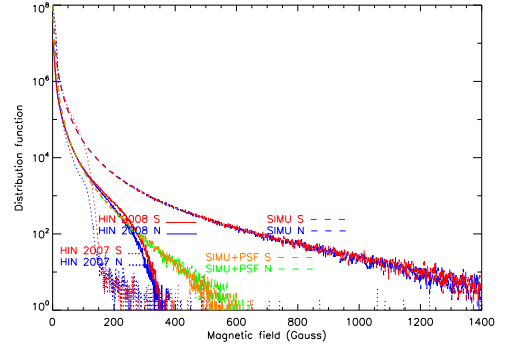


FIG. 5. Distribution functions of magnetic polarities (blue/red for north/south polarities); solid line: *Hinode* 2008, Na I D1; dotted line: *Hinode* 2007, Fe I; dashed line: simulation. The green/yellow curves (North/South) are for the simulation filtered by the SOT PSF.

ule of the 2D spatial Fourier transform averaged over the sequence duration and integrated over circular coronas. Power spectra of horizontal velocities computed from the LCT are in full agreement at the supergranular (30 Mm) and mesogranular (5 Mm) scales for observations and simulation. The power spectrum of the plasma velocity of the simulation (convolved by the temporal and spatial LCT windows) also agrees with LCT results. The filtering windows make the power spectra of horizontal velocities vanish at the granular scale (1 Mm); of course, this is not the case for plasma velocities of the simulation.

## VIII. GRANULE MERGING AND SPLITTING RATES

Splitting or exploding granules produce mesoscale horizontal flows and form families. We determined the splitting rate (fraction of exploding granules) and merging rate (fraction of collapsing granules) in BFI observations and simulation as a function of time. We did not find any significant time variation during the 24-hour sequences: the merging rate is 0.065 for the simulation (0.11 for *Hin-*

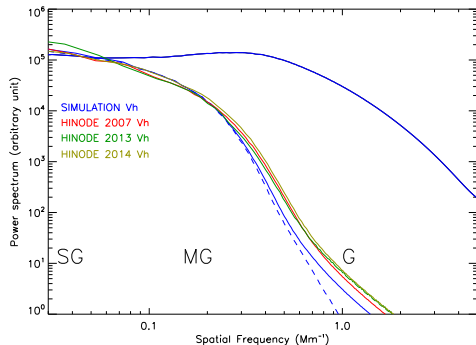


FIG. 6. Power spectra of horizontal velocities of observations and simulation. LCT velocities of observations: 2007 (red), 2013 (green), 2014 (dark green). Horizontal velocities of the simulation (blue): plasma velocity (thick), LCT velocity (thin) and plasma velocity after convolution by LCT windows (dashed). SG, MG and G designate typical supergranular, mesogranular and granular length scales.

ode 2007). The splitting rates are always higher: 0.115 for the simulation (0.14 for *Hinode* 2007). Splitting rates are always higher than merging rates; this explain the formation of TFG which appear both in observation and simulation and will be analysed in the next section.

### IX. DYNAMICS OF TREES OF FRAGMENTING GRANULES (TFG)

In paper I, we described the main properties of TFG. Their areas grow by a succession of granule explosions (some can occur simultaneously). TFG are able to push magnetic elements of the internetwork (IN) towards the frontiers of supergranules to form the network (NE). Explosions of granules at the TFG birth generate flows at the mesogranular scale in the range 0.5 to 0.8 km/s, which propagate outwards when there is no counterpart flow of adjacent families. We also evidenced the existence of large velocity fronts affecting the NE shape. Magnetic features are often located at the edge of such fronts.

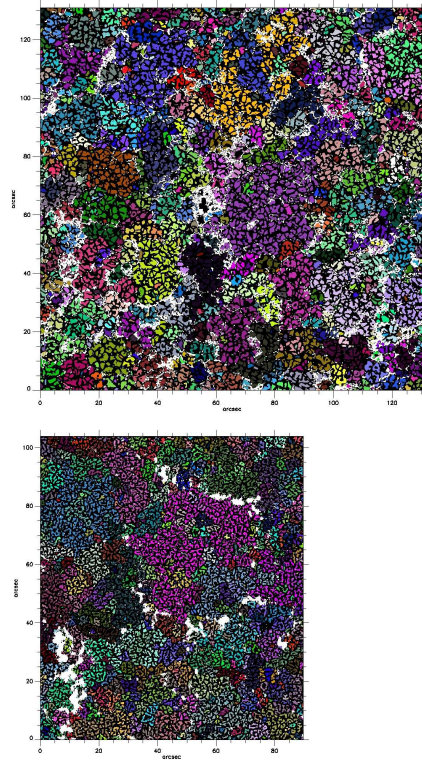


FIG. 7. TFG at maximum extension (top: simulation; bottom: *Hinode* 2007). Granules belonging to the same family have the same color. Magnetic fields (absolute value) are superimposed in white.

We discovered that TFG also form in the MHD simulation. Figure 7 displays TFG at the development time of the largest family (30'' or supergranular size), with the absolute value of BLOS superimposed. Magnetic fields are slowly advected to the borders of families, in observations and simulation, while new magnetic elements (located in intergranules) appear in the IN.

We now compare main characteristics of families using observations (2007, 2013 and 2014) and numerical results. Figure 8 shows that the distribution function of family lifetimes is typically a power law of the form  $t^{-1.88}$ , where  $t$  is the time. Most families develop to the mesoscale and have short lifetime (a few hours), while some rare TFG may last 24 hours or more and grow almost to the supergranular scale. The simulation appears in remarkable agreement with *Hinode*.

We also examined the distribution functions of the surface of families, and found a typical power law of the form  $t^{-1.74}$  (Figure 9). The maximum size corresponds to the supergranular scale: 28-29'' for the simulation and *Hinode* 2007, 18-20'' for 2013 and 2014. However, large families are not numerous: only ten families have areas in the range 500-900  $\text{arcsec}^2$  in the simulation; for 2007

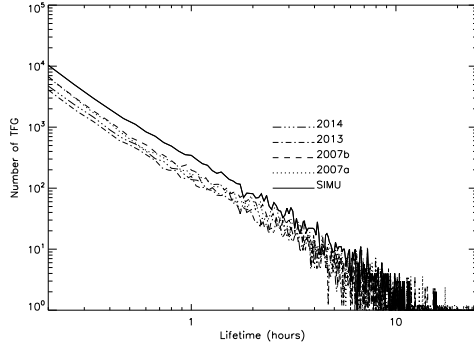


FIG. 8. Distribution of TFG lifetimes: *Hinode* observations of 2007, 2013 and 2014: dashed/dotted lines; simulation: solid line.

observations, the ten largest families are in the range  $300\text{--}900 \text{ arcsec}^2$ . Most supergranules appear rather formed of several families at the mesoscale ( $8''$  typical size): in a unit area of  $1' \times 1'$ , we found 113 families in the simulation above  $8''$  and 80 in observations (whatever the date).

Figure 10 shows the contribution of families to the FOV for two different lifetime thresholds as a function of time. Families lasting at least 3 hours represent 75 to 85 % of the FOV, while long life families (lasting more than 12 hours) cover 20 to 45% of the solar surface (the dispersion is higher because the number of long duration families is small).

Hence, we conclude that the spatio temporal properties of TFG as seen by *Hinode* or issued from the simulation fit well.

We noticed that the largest TFG are the most dynamic. Mean and maximum horizontal velocities of families are reported in Figure 11 as a function of their maximum area. For observations, velocities are derived from the LCT; for the simulation, we used both LCT and plasma velocities (filtered by LCT windows). While average velocities do not vary much with family area, velocity maxima increase with size. We conclude that strongest flows are generated by largest families composed of many

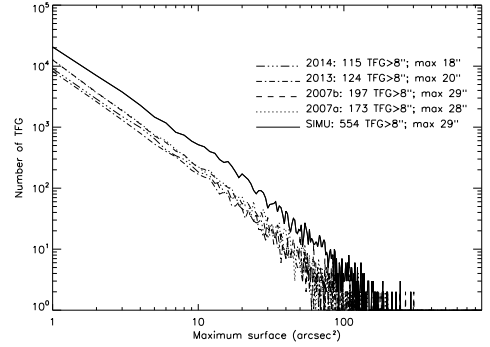


FIG. 9. Distribution of TFG sizes: *Hinode* observations of 2007, 2013 and 2014: dashed/dotted lines; simulation: solid line.

simultaneously exploding granules. Results are similar for *Hinode* and the MHD code.

Movies 1 and 2 display interactions between horizontal flows and BLOS for 2007 observations and simulation. Velocity fronts contribute to transport magnetic fields towards the boundaries of supergranules delineated by the NE. Strongest fronts occur at the border of large families, as shown in movies 3 and 4, suggesting that the dynamics of largest (but not numerous) TFG could play an important role in the NE buildup.

The NE formation at supergranular scale is illustrated (Figure 12) by the displacements of free corks, for *Hinode* 2007 as well as for the simulation. At time  $t = 0$ , corks were uniformly distributed on a regular grid. After initial time, corks move at the horizontal velocity of the LCT, and their trajectories are drawn. Final positions coincide with the magnetic network and delineate the boundaries of supergranules. We found, here again, an impressive agreement between observations and simulation. Movies 5 and 6 display the density of corks as a function of time, showing that corks are pushed towards the magnetic NE (which also correspond to bright He II  $30.4 \text{ nm}$  hot structures of *Hinode*/EIS 2007).

Cork motions can be characterized by a coefficient  $\gamma$  assuming that the square of the distance  $d^2$  from the initial



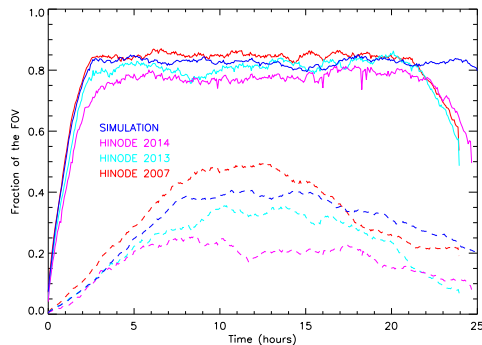


FIG. 10. Fraction of the FOV covered by families lasting more than 3 hours (solid lines) or more than 12 hours (dashed lines): simulation (blue), 2007 (red), 2013 (cyan) and 2014 observations (magenta).

position to the final position has the form of the power law  $t^\gamma$ . For pure diffusion or random motion,  $\gamma$  is about 1, but for advective motions,  $\gamma$  is higher. The LCT suppresses systematically Brownian motion, so that it does not appear in observations. On the contrary, this component is obvious in the simulation and is superimposed to the shift towards the NE. We computed the mean  $\gamma$  coefficient of observations and simulation. We found the following results.

1. Simulation: plasma velocity at  $0.13''$ , time step 60 seconds:  $\gamma = 1.02$  (Brownian motion dominates)
2. Simulation: plasma velocity at  $3.5''$ , time step 30 minutes:  $\gamma = 1.59$  (advection dominates)
3. LCT ( $3.5''$ , time step 30 minutes):
  - Simulation:  $\gamma = 1.82$
  - BFI 2007:  $\gamma = 1.66$
  - BFI 2013:  $\gamma = 1.67$
  - BFI 2014:  $\gamma = 1.64$

The  $\gamma$  values provided by the LCT for various datasets are in good agreement. After a few hours,  $\gamma$  decreases

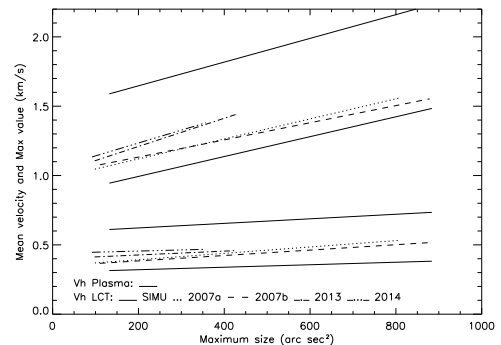


FIG. 11. Mean (bottom) and maximum (top) horizontal velocities. Simulation: velocity plasma filtered by the SOT PSF (thick line) and LCT (thin line); observations: 2007 (2 sequences, dashed and dotted), 2013 (dash dot) and 2014 (dash dot dot).

because corks have formed the NE, as shown by movies 5 and 6 where the surface density of corks is plotted. When corks reach cell boundaries, they slowly drift along them and tend to collapse together at particular points which correspond to intersections of several supergranules. This phenomenon is more visible in observations (movie 5) than in the simulation (movie 6) where the magnetic NE is more diffuse. Our results can be related to those of Giannattasio et al (2014a and 2014b) based on NFI magnetograms in Na I D1 line: they found 1.44 for magnetic element displacements and 1.55 for magnetic pairs. However, corks are not magnetic elements; they move freely at the speed of the plasma flow.

## X. DISCUSSION

The surface of the Sun is covered by solar granules which are grouped in TFG or families. We used continuum intensities to evidence and label exploding granules forming families. The BFI provided intensities at 450 nm, but synthetic emergent intensities are at 500 nm.



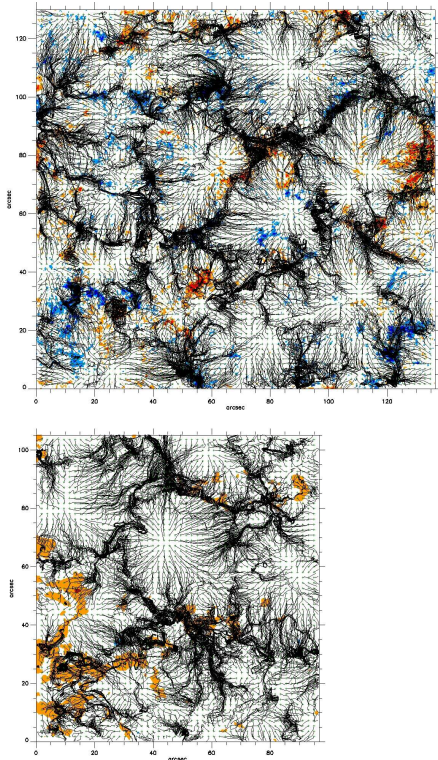


FIG. 12. Trajectories of corks. Initial positions are indicated by green crosses. Magnetic polarities (green/blue and yellow/red) are superimposed. Top: simulation; bottom: *Hinode* 2007

Danilovic *et al.* (2008) compared granulation contrast seen by the *Hinode* spectro polarimeter (SP) with MHD simulation and found that, at 630 nm, the simulated contrast decreases from 0.14 to 0.07 after applying the SOT PSF (close to the observed value). Wedemeyer-Böhm and Rouppe van der Voort (2009) compared BFI images in the blue (450 nm), green (555 nm) and red (668 nm) continua to synthetic images degraded by the PSF and found 0.11 in the blue. In the present study, the BFI contrast at 450 nm is 0.13. Granulation images of the simulation have a contrast of 0.155 at 500 nm, reducing to 0.105 after filtering by the SOT PSF. We found that the recognition of TFG is little affected by the PSF because granule evolution between two consecutive times relies on the detection of a common surface. The PSF removes the small granules or details but does not affect the formation of TFG, which are built essentially by the middle and large size granules (although some branches may be cut). This is why we discovered recently (work still in progress) that TFG are still detected at the SDO HMI resolution.

Averaged horizontal velocities were computed by the LCT through windows of 30 minutes and  $3.5''$ ; using the

simulation, we found a good agreement between the LCT applied to continuum images and plasma motion except that the velocity module is underestimated by a factor two. Using another simulation, Verma *et al.* (2013) showed that the LCT recovers main features of the granulation dynamics, but proper motions may be underestimated by factor of three. Louis *et al.* (2015) have also compared this technique to simulated flow fields and concluded that LCT is a viable and fast tool to retrieve velocities for large data sets, with good correlation between vectors and underestimation of the magnitude. Alternative methods are discussed by Welsch *et al.* (2007). Recently, Asensio Ramos *et al.* (2017) developed a new algorithm (DeepVel) working on consecutive images to evidence small scale instantaneous motions, but providing similar results to LCT for averaged velocity fields.

TFG sizes are distributed continuously with a decreasing slope from small (mesoscale) to large (supergranule); this is also the case of lifetimes. TFG compete each other but largest ones, which are not numerous (power law), generate the strongest horizontal flows pushing the IN magnetic field to the border of supergranules to form the quiet NE. Thus, TFG appear as an essential part of the supergranulation. This schematic view of TFG dynamics is compatible with the evolution of the IN and maintenance of the NE described by Gošić *et al.* (2014). They evidenced, using NFI observations in Na I D1, a flux transfer from the IN to the NE, supplying as much flux as present in the NE in 24 hours. We report here large scale horizontal flows generated by the TFG irrespective to the date along the solar cycle (2007, 2013 and 2014) and suggest that their associated flows could contribute to the transport of magnetic elements from the IN to the NE.

## XI. CONCLUSION

We have studied the dynamics of the quiet Sun from disk center observations of the *Hinode* SOT in terms of mesoscale horizontal flows, evolution of TFG (trees of fragmenting granules or families) and line of sight magnetic fields, along the cycle (2007 at solar minimum, 2013 and 2014 near solar maximum) using 24-hour sequences; results were compared to those issued from the magneto-convection code at similar space and time resolutions after filtering by the SOT PSF. Horizontal flows in observations were computed using the LCT applied to intensities; for the simulation, we used both LCT and plasma velocity and found good agreement with *Hinode*. In all cases, TFG appear after a few hours, most at the mesoscale, but some (composed of several branches) reach the supergranular scale. Families are associated to velocity fronts which advect magnetic fields and contribute to form the network. Largest TFG are not numerous but the most dynamic; their development could be an efficient mechanism to build the network. The simulation provides realistic results about the properties, dynamics of TFG

and network interaction. However, small discrepancies do exist, as granule merging/splitting rates or magnetic field polarities which appear more mixed in the simulation than in observations (although this may come from instrumental effects and remnant activity).

We do not see any striking variation of the dynamics between solar minimum and maximum, confirming a previous study by Roudier *et al.* (2017) based on SDO/HMI observations. However, we need to analyze more data between 2007 and 2013 in the ascending phase, but unfortunately the number of exploitable sequences at disk center in the blue continuum is rather limited. G band sequences are more frequent but also more difficult to analyze with the LCT (bright points). We checked that IRIS observations (slit jaw continuum at 283 nm) are LCT compatible, so that new data could be used in the future to cover longer periods along the cycle. For that purpose, HOP312 with IRIS has been set up.

The Electronic Supplemental Material movies are available in MP4 format.

- Movie 1: horizontal velocities ( $\sqrt{v_x^2 + v_y^2}$ ) of *Hinode*/BFI from LCT of blue continuum, 29-31 August 2007, sequence duration 48 hours, FOV  $65'' \times 75''$ . Velocities in grey levels (LCT windows of 30 minutes/3.5''). The line of sight magnetic field (Stokes  $V$  as a proxy of BLOS from *Hinode*/NFI blue wing of FeI 630.2 nm, pixel size  $0.16''$ , 5 minutes averaged) is shown in blue/orange for North/South polarities.
- Movie 2: horizontal plasma velocities averaged through 30 minutes/3.5'' filters (LCT windows for comparison with movie 1) of the numerical simulation, sequence duration 26 hours, FOV  $131'' \times 131''$ . Velocities in grey levels. The vertical component of the magnetic field (pixel size  $0.13''$ , 5 minutes averaged) is superimposed in blue/orange for north/south polarities.
- Movie 3: Families of granules (TFG in various colors) derived from *Hinode*/BFI blue continuum at 450.4 nm, 29-31 August 2007, sequence duration 48 hours, FOV  $90'' \times 105''$ , pixel size  $0.11''$ , together with horizontal velocities from LCT technique (30 minutes/3.5'' windows, grey levels).
- Movie 4: Families of granules (TFG in various colors) provided by the numerical simulation, sequence duration 25 hours, FOV  $131'' \times 131''$ , pixel size  $0.13''$ , together with horizontal plasma velocities (grey levels, 30 minutes and 3.5'' filtered

through LCT windows for comparison with movie 3).

- Movie 5: density of corks (initially uniformly distributed over the FOV) represented by disks (size proportional to corks number, 10, 30, 100, 300, 1000, 3000 and 10000 or more). The corks are driven by horizontal LCT velocities (30 minutes/3.5'' windows) from *Hinode*/BFI blue continuum at 450.4 nm, 29-31 August 2007, sequence duration 48 hours, FOV  $90'' \times 105''$ . BLOS (*Hinode*/NFI blue wing of FeI 630.2 nm) is superimposed in blue/red for north/south polarities. In the background, HeII 30.4 nm intensities from *Hinode*/EIS are displayed in green.
- Movie 6: density of corks of simulation represented by disks (size proportional to the number of corks). The corks are driven by horizontal plasma velocities, sequence duration 26 hours, FOV  $131'' \times 131''$ . The vertical magnetic field is superimposed in blue/orange for north/south polarities. The time step is 10 minutes and the averaging window 3.5'' (to allow comparison with movie 5).

## ACKNOWLEDGMENTS

We are indebted to the *Hinode* team for the possibility to use their data. *Hinode* is a Japanese mission developed and launched by ISAS/JAXA, collaborating with NAOJ as a domestic partner, NASA and STFC (UK) as international partners. Scientific operation of the *Hinode* mission is conducted by the *Hinode* science team organized at ISAS/JAXA. This team mainly consists of scientists from institutes in the partner countries. Support for the post-launch operation is provided by JAXA and NAOJ (Japan), STFC (UK), NASA, ESA, and NSC (Norway).

The authors wish to acknowledge the anonymous referee and the editor for helpful comments and suggestions to improve the manuscript.

Computing resources for the simulations were provided by the NASA High-End Computing Program through the NASA Advanced Supercomputing Division at the Ames Research Center.

This work was also supported by the Centre National de la Recherche Scientifique, France. We acknowledge access to the HPC resources of CALMIP under the allocation 2011-P1115.

\* Jean-Marie.Malherbe@obspm.fr

† Thierry.Roudier@irap.omp.eu

‡ Stein@pa.msu.edu

§ Zoe@lmsal.com

<sup>1</sup> Asensio Ramos, A., Requerey, I., Vitas, N.: 2017, *Astron. Astrophys.*, **604**, 11. DOI: 10.1051/0004-6361/201730783

- <sup>2</sup> Asplund, M., Nordlund, Å., Trampedach, R., Allende Prieto, C., Stein, R. F. : 2000, *Astron. Astrophys.*, **359**, 743
- <sup>3</sup> Carlsson, M., Stein, R. F., Nordlund, Å., Scharmer, G. B. : 2004, *Astrophys. J.*, **610**, 137, DOI:10.1086/423305
- <sup>4</sup> Danilovic, S., Gandorfer, A., Lagg, A., Schüssler, M., Solanki, S., Vögler, A., Katsukawa, Y., Tsuneta, S.: 2008, *Astron. Astrophys.*, **484**, L17. DOI: 10.1051/0004-6361/200809857.
- <sup>5</sup> De Pontieu, B., Carlsson, M., Stein, R., Rouppe van der Voort, L., Löfdahl, M., van Noort, M., Nordlund, Å., Scharmer, G.: 2006, *Astrophys. J.*, **646**, 1404, DOI:10.1086/505074
- <sup>6</sup> Dominguez Cerdeña, I., Sanchez Almeida, J., Kneer, F.: 2006, *Astrophys. J.*, **646**, 1421. DOI: 10.1086/505129.
- <sup>7</sup> Fisher, G., Welsch, B.: 2008, *ASP Conf. Series*, **383**, 373.
- <sup>8</sup> Georgobiani, D., Zhao, J., Kosovichev, A., Benson, D., Stein, R., Nordlund, Å.: 2007, *Astrophys. J.*, **657**, 1157. DOI: 10.1086/511148.
- <sup>9</sup> Giannattasio, F., Berrilli, F., Biferak, L., Del Moro, D., Sbragaglia, M., Bellot Rubio, L., Gošić, M., Orozco Suárez, D.: 2014a, *Astron. Astrophys.*, **569**, 121. DOI: 10.1051/0004-6361/201424380.
- <sup>10</sup> Giannattasio, F., Strangalini, M., Berrilli, F., Del Moro, D., Bellot Rubio, L.: 2014b, *Astrophys. J.*, **788**, 137. DOI: 10.1088/0004-637X/788/2/137.
- <sup>11</sup> Gošić, M., Bellot Rubio, L., Orozco Suárez, D., Katsukawa, Y., del Toro Iniesta, J.C.: 2014, *Astrophys. J.*, **797**, 49. DOI: 10.1088/0004-637X/788/1/49.
- <sup>12</sup> Ichimoto, K., Tsuneta, S., Suematsu, Y., Shimizu, T., Otsubo, M., Kato, Y., *et al.*: 2005, In: Mather, J. C. (ed.), *Optical, Infrared, and Millimeter Space Telescopes, Proc. SPIE* **5487**, 1142.
- <sup>13</sup> Langangen, O., Carlsson, M., Rouppe van der Voort, L., Stein, R.: 2007, *Astrophys. J.*, **655**, 615, DOI:10.1086/509754
- <sup>14</sup> Louis, R., Ravindra, B., Georgoulis, M., Küker, M.: 2015, *Solar Phys.* **290**, 1135. DOI: 10.1007/s11207-015-0659-2.
- <sup>15</sup> Malherbe, J.M., Roudier, T., Frank, Z., Rieutord, M.: 2015, *Solar Phys.* **290**, 321. DOI: 10.1007/s11207-014-0630-7.
- <sup>16</sup> November, L.J., Simon, G.W.: 1988, *Astrophys. J.* **333**, 427. DOI: 10.1086/166758.
- <sup>17</sup> Orozco Suárez, D., Bellot Rubio, L., Del Toro Iniesta, J.C.: 2007, *Astrophys. J.*, **662**, L31, DOI:10.1086/519279
- <sup>18</sup> Ossendrijver, M.: 2003, *Astron. Astrophys. Rev.* **11**, 287. DOI: 10.1007/s00159-003-0019-3.
- <sup>19</sup> Rieutord, M., Roudier, T., Ludwig, H., Nordlund, A., Stein, R.: 2001, *Astron. Astrophys.* **377**, 14. DOI: 10.1051/0004-6361:20011160.
- <sup>20</sup> Rieutord, M., Roudier, T., Roques, S., Ducottet, C.: 2007, *Astron. Astrophys.* **471**, 687. DOI: 10.1051/0004-6361:20066491.
- <sup>21</sup> Rosenthal, C. S., Christensen-Dalsgaard, J., Nordlund, Å., Stein, R. F., Trampedach, R. : 1999, *Astron. Astrophys.*, **351**, 689
- <sup>22</sup> Roudier, T., Rieutord, M., Malherbe, J.-M., Vigneau, J.: 1999, *Astron. Astrophys.* **349**, 301.
- <sup>23</sup> Roudier, T., Lignières, F., Rieutord, M., Brandt, P.N., Malherbe, J.M.: 2003, *Astron. Astrophys.* **409**, 299. DOI: 10.1051/0004-6361:20030988.
- <sup>24</sup> Roudier, T., Rieutord, M., Brito, D., Rincon, F., Malherbe, J.M., Meunier, N., Berger, T., Frank, Z.: 2009, *Astron. Astrophys.* **495**, 945. DOI: 10.1051/0004-6361:200811101.
- <sup>25</sup> Roudier, T., Rieutord, M., Malherbe, J.M., Renon, N., Berger, T., Frank, Z., Prat, V., Gizon, L., Svanda, M.: 2012, *Astron. Astrophys.* **540**, 88.
- <sup>26</sup> Roudier, T., Malherbe, J.M., Rieutord, M., Frank, Z.: 2016, *Astron. Astrophys.* **590**, 121. DOI: 10.1051/0004-6361/201628111.
- <sup>27</sup> Roudier, T., Malherbe, J.M., Mirouh, G.M.: 2017, *Astron. Astrophys.* **598**, 99. DOI: 10.1051/0004-6361/201629274.
- <sup>28</sup> Sheeley, N.R.: 2005, *Living Rev. Solar Phys.*, **2**, 5. DOI: 10.12942/lrsp-2005-5.
- <sup>29</sup> Stein, R., Nordlund, Å.: 1998, *Astrophys. J.*, **499**, 914. DOI: 10.1086/305678.
- <sup>30</sup> Stein, R., Nordlund, Å.: 2000, *Astrophysical turbulence and convection*, J. Buchler and H. Kandrup Eds., Annals N.Y. Acad. Sci., **898**, 21-38.
- <sup>31</sup> Stein, R., Nordlund, Å.: 2000, *Solar Phys.*, **192**, 91. DOI: 10.1023/A:1005260918443.
- <sup>32</sup> Stein, R., Nordlund, Å.: 2001, *AstroPhys. J.*, **546**, 585. DOI: 10.1086/318218
- <sup>33</sup> Stein, R., Lagerfjård, A., Nordlund, Å., Georgobiani, D., Benson, D., Schaffenberger, W.: 2009, *ASP Conf. Series*, **415**, 63.
- <sup>34</sup> Stein, R.: 2012, *Living Rev. Solar Phys.*, **9**, 4. DOI:10.12942/lrsp-2012-4
- <sup>35</sup> Suematsu, Y., Tsuneta, S., Ichimoto, K., Shimizu, T., Otsubo, M., Katsukawa, Y., *et al.*: 2008, *Solar Phys.* **249**, 197. DOI: 10.1007/s11207-008-9129-4.
- <sup>36</sup> Title, A., Tarbell, T., Topka, K., Ferguson, S., Shine, R.: 1989, *Astrophys. J.* **336**, 475. DOI: 10.1086/167026.
- <sup>37</sup> Verma, M., Steffen, M., Denker, C.: 2013, *Astron. Astrophys.*, **555**, 136. DOI: 10.1051/0004-6361/201321628
- <sup>38</sup> Wedemeyer-Böhm, S., Rouppe van der Voort, L.: 2009, *Astron. Astrophys.*, **503**, 225. DOI: 10.1051/0004-6361/200911983
- <sup>39</sup> Welsch, B., DeRosa, M., Fisher, G., Georgoulis, M., Kusano, K., Longcope, D., Ravindra, B., Schuck, P.: 2007, *Astron. Astrophys.*, **670**, 1434. DOI: 10.1086/522422
- <sup>40</sup> Zhao, J., Georgobiani, D., Kosovichev, A., Benson, D., Stein, R., Nordlund, Å.: 2007, *Astrophys. J.*, **659**, 848, DOI: 10.1086/512009